

TOWARD END-TO-END SEISMIC SIMULATIONS FOR NUCLEAR EXPLOSION MONITORING

Arthur J. Rodgers¹, Oleg Y. Vorobiev², N. Anders Petersson³, Bjorn A. Sjögreen³, and Megan Avants¹

Lawrence Livermore National Laboratory¹, Computational Geosciences Group², and
the Center for Advanced Scientific Computing³

Sponsored by the National Nuclear Security Administration

Award No. DE-AC52-07NA27344/LL09-Simulation-NDD02

ABSTRACT

This paper describes new research being performed to improve understanding of seismic waves generated by underground nuclear explosions (UNE) by using full waveform simulation, high-performance computing and three-dimensional (3D) earth models. The goal of this effort is to develop an end-to-end modeling capability to cover the range of wave propagation required for nuclear explosion monitoring (NEM) from the buried nuclear device to the seismic sensor. The goal of this work is to improve understanding of the physical basis and prediction capabilities of seismic observables for NEM including source and path-propagation effects. We are pursuing research along three main thrusts. Firstly, we are modeling the non-linear hydrodynamic response of geologic materials to underground explosions in order to better understand how source emplacement conditions impact the seismic waves that emerge from the source region and are ultimately observed hundreds or thousands of kilometers away. Empirical evidence shows that the amplitudes and frequency content of seismic waves at all distances are strongly impacted by the physical properties of the source region (e.g., density, strength, porosity). To model the near-source shock-wave motions of an UNE, we use GEODYN, an Eulerian Godunov (finite volume) code incorporating thermodynamically consistent non-linear constitutive relations, including cavity formation, yielding, porous compaction, tensile failure, bulking and damage. In order to propagate motions to seismic distances we are developing a one-way coupling method to pass motions to WPP (a Cartesian anelastic finite difference code). Preliminary investigations of UNE's in canonical materials (granite, tuff and alluvium) confirm that emplacement conditions have a strong effect on seismic amplitudes and the generation of shear waves.

Specifically, we find that motions from an explosion in high-strength, low-porosity granite have high compressional wave amplitudes and weak shear waves, while an explosion in low strength, high-porosity alluvium results in much weaker compressional waves and low-frequency compressional and shear waves of nearly equal amplitude. Further work will attempt to model available near-field seismic data from explosions conducted at the Nevada Test Site (NTS), where we have accurate characterization of the sub-surface from the wealth of geological and geophysical data from the former nuclear test program. Secondly, we are modeling seismic wave propagation with free-surface topography in WPP. We have modeled the October 9, 2006, and May 25, 2009, North Korean nuclear tests to investigate the impact of rugged topography on seismic waves. Preliminary results indicate that the topographic relief causes complexity in the direct *P*-waves that leads to azimuthally dependent behavior and the topographic gradient to the northeast, east and southeast of the presumed test locations generate stronger shear-waves, although each test gives a different pattern. Thirdly, we are modeling intermediate period motions (10–50 seconds) from earthquakes and explosions at regional distances. For these simulations we run SPEC-FEM3D_GLOBE (a spherical geometry spectral element code). We modeled broadband waveforms from well-characterized and well-observed events in the Middle East and central Asia, as well as the North Korean nuclear tests. For the recent North Korean test we found that the one-dimensional iasp91 model predicts the observed waveforms quite well in the band 20–50 seconds, while waveform fits for available 3D earth models are generally poor, with some exceptions. Interestingly 3D models can predict energy on the transverse component for an isotropic source presumably due to surface wave mode conversion and/or multipathing.

OBJECTIVES

Advances in numerical methods, improvements in the power and availability of high-performance computing and improved data and methods to estimate three-dimensional (3D) earth models for wave propagation makes it possible to simulate seismic waves with resolution relevant to NEM. This effort seeks to realize the goal of end-to-end simulation of seismic waves from UNE's. Specifically we are working to apply numerical methods for wave propagation to enable simulation of seismic waves from the near-source (shock wave) regime, through the heterogeneous earth to the seismic sensor. The ultimate goal of this research is to improve estimates of explosion size and confidence in source type discrimination by using simulations of seismic waveforms and observables and their uncertainties including both source and path propagation effects. Applications include post-event analysis and predictions for possible future nuclear tests in regions where little or no empirical data are available.

The three thrusts of this study are aimed to address one or more challenges of NEM. Shock wave modeling aims to improve understanding of the effects of emplacement conditions on yield and source-type estimates. Elastic modeling in the presence of surface topography aims improve understanding of how rough topography distorts *P*- and excites *S*-waves (body and surface waves) emerging from shallow explosions to improve prediction of amplitude and *P*-to-*S* partitioning. Finally, intermediate-period regional-complete waveform modeling aims to improve prediction of waveforms and understanding of the biases in source estimates due to path propagation effects.

RESEARCH ACCOMPLISHED

This paper describes several ongoing efforts that are unified in their goal of developing an end-to-end (device-to-detector) capability for modeling seismic waves from UNE's. Simulation of seismic waves from UNE's requires modeling the behavior of earth materials in different regimes. Hydrodynamic methods must be employed to model the shock wave emerging from the device and propagating to distances beyond which the motions are elastic. These methods are computationally expensive and require very fine spatial and temporal discretization. This is contrasted by the fact that weakly anelastic propagation methods are computationally more efficient than (non-linear) hydrodynamic methods and are appropriate for most of the path-length. A common theme is that the numerical methods used for modeling wave propagation must rely on high-performance computing to realize simulations to the distances (computational domain size) and desired resolution (i.e., target frequencies and wavelengths of NEM). Furthermore, methods must be general enough to simulate wave propagation in realistic 3D earth models, where material properties vary in each spatial dimension possibly across a broad spectrum of wavelengths. In this paper we report progress along three thrusts: 1) modeling the near-source region of a UNE with emphasis on the hydrodynamic response of geologic media and propagation to seismic distances; 2) modeling of anelastic wave propagation in the presence of free-surface topography; and 3) modeling of intermediate period (10–50 seconds) complete waveforms at regional distances.

Modeling Shock Waves Generated by UNE's and Coupling GEODYN to WPP

We are modeling shock wave propagation in the near-source region with GEODYN, an Eulerian Godunov (finite volume) code incorporating thermodynamically consistent non-linear constitutive relations, including cavity formation, yielding, porous compaction, tensile failure, bulking and damage (Antoun et al., 2001; Antoun and Lomov, 2003; Lomov et al., 2003). This code models the high energy density region near the source and the propagation of the shock wave into the weakly anelastic regime. We validated the code and our material models by comparing the simulation results against available experimental data. In order to propagate motions to seismic distances we are developing a one-way coupling method to pass motions to WPP, a Cartesian anelastic finite difference code developed at LLNL (Nilsson et al., 2007).

Preliminary investigations of UNE's in canonical materials confirm that emplacement conditions have a strong effect on seismic amplitudes and on the generation of shear waves. Figure 1a shows peak velocities (data points) as a function of scaled distance for UNE's for granite, tuff and alluvium as reported by Perret and Bass (1974). Also shown are peak velocities from GEODYN simulations (solid lines). The scaled range is taken as the slant distance divided by the explosive yield to the 1/3 power. Note that the peak velocities are largest for granite, then tuff, then alluvium and the scaled range extends beyond the nominal elastic radius. The differences between peak motions for different materials at a given scaled distance are quite significant, up a factor of ten. While there is scatter in the observational data and the granite data do not span a large range, the simulations provide a reasonably good fit to the

experimental data. This gives us confidence that GEODYN simulations and our material models can accurately model near-source motions in the regions of both non-linear and linear behavior.

In another more specific validation exercise we compared peak displacements from a series of chemical high-explosive (HE) experiments in limestone performed in Kirghizia in 1960 (Murphy et al., 1997). The generic strength model described in Vorobiev (2008) was used in GEODYN to model limestone with 0.5% porosity. In situ experimental measurements of ground motion at different distances from the shot point were reported by Murphy et al. (1997). The explosions and motion recordings reported in this study were conducted in the subsurface in essentially rock whole-space conditions, making them ideal for our simulation validation experiments.

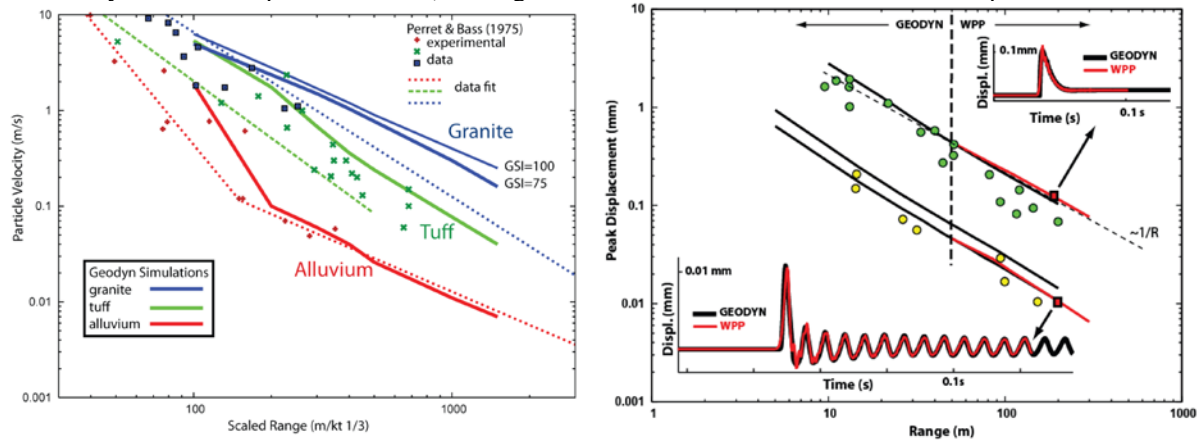


Figure 1. (a, left) Peak velocities as a function of scaled distance for UNE's in granite (blue), tuff (green) and alluvium (red). The symbols indicate observed values from Perret and Bass (1974) and the solid lines are from GEODYN simulations. (b, right) Peak displacements as a function of range for experimental data (circles) from Murphy et al., (1997) and GEODYN calculations (black line). Also shown are the displacement time-histories (inset plots) from GEODYN (black lines) and from the one-way code coupling approach where motions were passed from GEODYN to WPP (red lines), propagated with both codes and compared at 200 m range (red square).

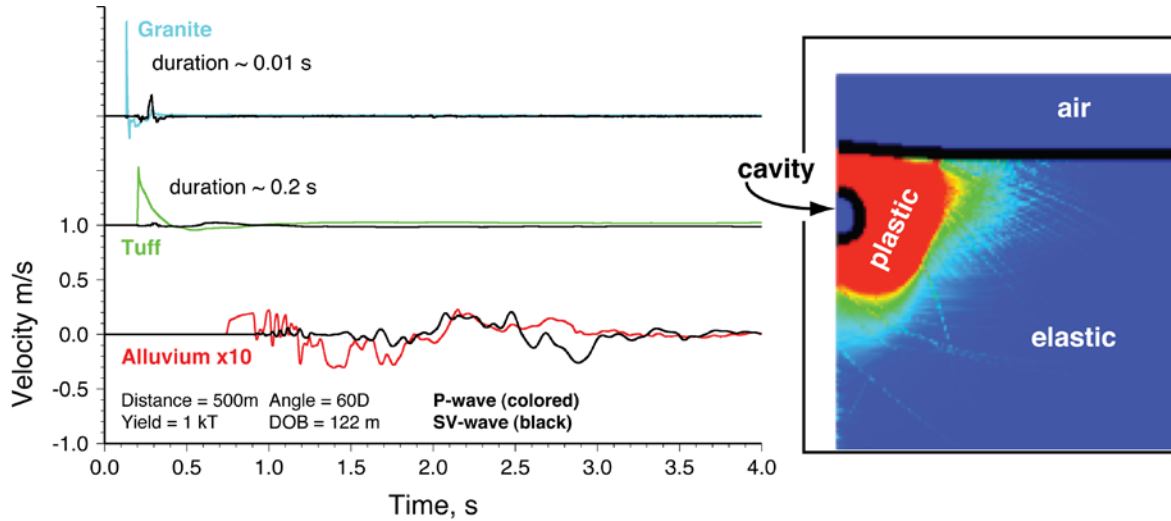


Figure 2. (a, left) *P*-wave velocity time-histories for 1 kT chemical explosions in granite (cyan), tuff (green) and alluvium (red). The corresponding *SV*-wave time-histories (black) on the same scale as the *P*-wave motions. Note that motions in alluvium are amplified by a factor of ten. (b, right) Post-event strain field for a 1 kT chemical explosion in granite at a normal scaled depth-of-burial (122 m): the inner circle indicates the cavity; red values indicate strains greater than 10^{-6} ; and darkest blue outside the cavity corresponds to elastic motions.

We performed a series of GEODYN simulations to investigate the effects of explosion emplacement conditions on ground motions. The simulations were performed in two-dimensions using a uniform solid material (granite, tuff or alluvium) overlain by air. We sampled the wavefield time-histories at a number of points and decomposed the motions into radial (*P*-wave) and vertically polarized transverse (*SV*-wave) motions. Figure 2a shows the decomposed velocity time-histories at a range of 500 m from the shot point (in the elastic region) at an angle of 60° from the vertical, corresponding to a teleseismic take-off angle. *P*- and *SV*-wave motions are shown together as colored and black seismograms, respectively. Notice the great difference in the arrival time, pulse duration and *P*-to-*SV* energy partitioning for the different materials. The shot in granite results in a fast arriving wave with very short duration (~0.01 s) while the shot in tuff arrives later with a longer duration (~0.2 s). The shot in alluvium results in much weaker motions (shown amplified by a factor of ten in Figure 2a) with more complexity and longer duration than the other materials. The differences in *P*-wave pulse width are also reflected in corner frequencies of amplitude spectra (not shown). Also note the differences in the relative *P*- and *SV*-wave amplitudes. The shot in alluvium generates 1 Hz *P*- and *SV*-wave energy of roughly equal amplitude. These differences in *P*- and *SV*-wave spectral amplitudes result in very different high-frequency *P*/*S* amplitude ratios used for event identification. Preliminary results (not shown) indicate simulated cross-spectral ratios (high-frequency *P* / low-frequency *S*) are consistent with observations from the NTS reported by Walter et al. (1995).

Similar to many other numerical methods for wave propagation, GEODYN allows us to sample the strains and record the peak strain at all points in the computational domain. Figure 2b shows the peak strain around the shot point for a 1 kT chemical shot in granite at the normal scaled depth-of-burial (122 m). The cavity is formed around the shot point and indicated by the inner semi-circle. Colors show the strain with red colors corresponding to plastic strains of 10^{-6} or greater and the darkest blue outside the cavity corresponding to elastic strains. Self-affine properties of the material strength causes the asymmetric pattern of strains (yellow to cyan colors) due to fracture.

In order to simulate seismic ground motions to distances where observations are typically made (> 1 km), we are coupling motions from GEODYN to our anelastic wave propagation code, WPP. This is a one-way coupling where we compute the response of the material in the non-linear regime through to the elastic regime. Motions are saved on a dense grid of points on the faces of a cube and passed to WPP as forcing on an internal surface. Figure 1b shows the results of modeling the experimental data in Murphy et al. (1997) for small chemical explosions in a limestone whole-space. Here we have passed the motions from GEODYN to WPP at a distance of 40 m and propagated motions in both codes to 200-300 m. The GEODYN calculation is extended into the linear elastic regime and results indicate that the peak displacements from both codes match the amplitudes versus range perfectly. Furthermore, the time-histories agree nearly perfectly indicating that numerical artifacts due to interpolation or grid dispersion are minimal. We are currently operationalizing this process to enable routine modeling of seismic motions to seismic distances.

Modeling the Effect of Topography on Seismic Waves from the 2006 and 2009 North Korean Nuclear Tests

We have developed and implemented a method to model free-surface topography with WPP. The rough surface is handled with a conforming grid that follows the topography above some depth, below which the usual Cartesian grid with mesh refinement is used. We have validated our implementation of topography in WPP with canonical solutions as well as compared motions from different implementations (e.g., finite element, hybrid finite element/finite difference) for earthquake scenarios in the San Francisco Bay Area (Aagaard et al., 2009). Note that WPP is open source and available at <https://computation.llnl.gov/casc/serpentine/index.html>.

The recent nuclear tests in North Korea provide a ready application for the investigation of the effects of topography on ground motions. We performed simulations of explosions on a 40-km domain around the test site. Figure 3a shows the topographic relief, estimated shot locations and computational domain (white outline). The depth of the shots was taken to be 600 m below the local topography of each event and an isotropic source was used. Note that the relief varies greatly near the shot points. The calculations used a purely elastic homogenous material model ($v_p = 5810$ m/s, $v_s = 3350$ m/s and $\rho = 2660$ kg-m/s). We show results from calculations with a grid spacing of 50 meters resolving motions above 4 Hz.

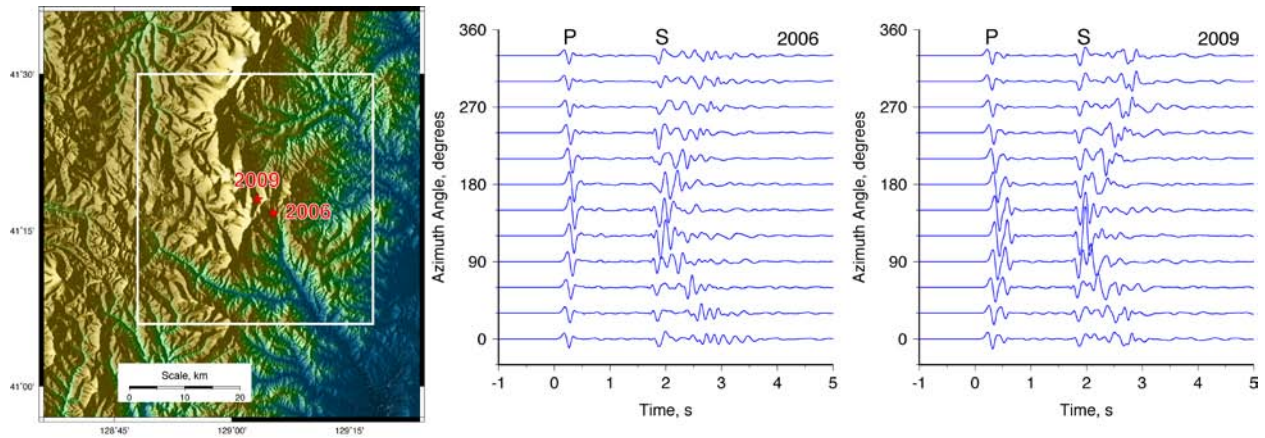


Figure 3. (a, left) Topographic relief in and around the North Korean nuclear test site along with locations of the 2006 and 2009 explosions. Also shown is the computation grid for WPP simulations with topography (white box). (b, center) Vertical displacement motions (down positive) aligned on the *P*-wave for locations below the 2006 explosion (60° from the vertical). (c, right) Same as (b) but for the 2009 explosion.

Figures 3b and 3c show the vertical displacement motions (down positive) below the 2006 and 2009 explosions at locations distributed azimuthally around the shot point at a take-off angle of 60° from the vertical corresponding to teleseismic *P*- and *S*-waves. The timing and particle motions of the time-histories clearly indicate the *P*- and *S*-wave packets marked in the figure. Note that the initial *P*-wave is different in character for the 2006 and 2009 events, with the 2006 event showing a simple compression and dilatation, while the *P*-waves from the 2009 event show a large amplitude compression following the initial compression-dilatation whose amplitudes are particularly strong at azimuths of 30°-150°. Both shots show strong azimuthal variations with the largest *P*- and *S*-wave amplitudes at azimuths of 90°-180°. Because the material model was homogeneous and the sources were identical, the differences in wave propagation behavior can only be attributed to interaction of the wavefield with the free surface and its variation for the different shot points. The variation in response is not surprising however given that the topography varies significantly on scales of the wavelengths of *P*- and *S*-waves in the band 1-4 Hz (1.4-5.6 km for *P*-waves and 0.8-3.4 km for *S*-waves) and on the order of the event separation (less than 5 km). These simulations suggest wave propagation in the presence of topographic relief can rapidly degrade waveform correlation for nearby explosions.

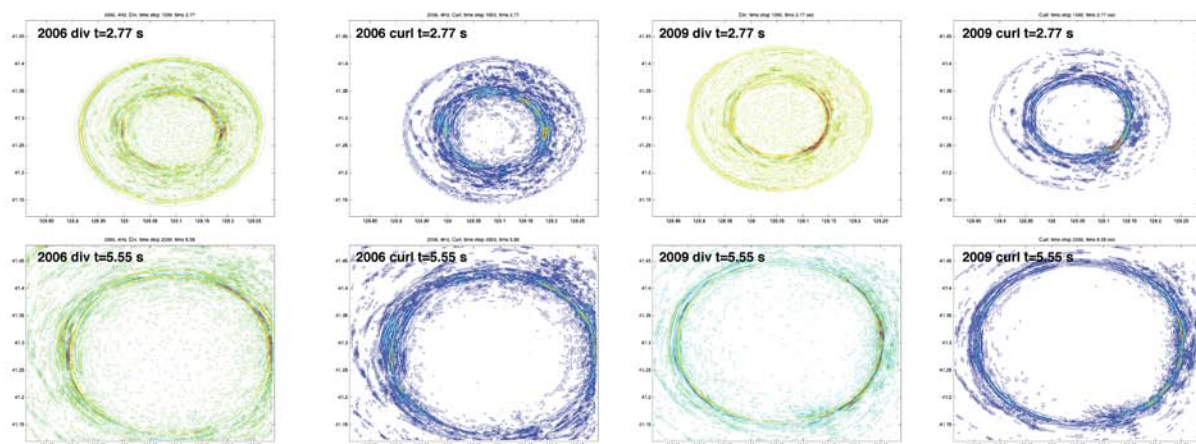


Figure 4. Motions at the surface at two different times (2.77 s and 5.55 s) for the 2006 (left) and 2009 (right) simulations. For each simulation we show the divergence and curl of the velocity field corresponding to the *P*- and *S*-wave motions. Note these are plotted in map view with some compression of the north-south directions.

Additional insight into the complexities of the wavefields emerging from these explosions can be seen in the images of the divergence and curl of the velocity fields at the surface, corresponding to *P*- and *S*-wave motions, respectively. Figure 4 shows the divergence and curl of the velocity field at the surface for the 2006 and 2009 explosions at two different times (2.77 s and 5.55 s). Similar to the seismograms shown above, the wavefields show strong azimuthal dependence. Especially interesting is the variation of the *P*- and *S*-wave amplitudes. The largest amplitudes for both *P*- and *S*-waves at early times for the 2006 event is to the east-to-northeast and west of the shot point, while the 2009 event shows strong amplitudes to the southeast-to-northeast. These azimuths also correspond to locally high topography and large variations in relief (measured by the topographic gradient or slope) relative to the shot point suggesting amplification by topographic highs and enhanced conversion of *P*-to-*S* propagation modes at topographic relief.

Theoretical studies based on incident plane-waves (Bouchon, 1973; Campillo and Bouchon, 1985; Sanchez-Sesma, 1983;) and elastic finite difference (FD) modeling (Boore; 1972) showed that topography impacts seismic motions when the seismic wavelength is comparable to the size of topographic features. These studies indicated that motions are amplified at topographic peaks and de-amplified in valleys. Chaljub (2006) showed that amplification occurs at topographic highs around the Grenoble alpine valley using the spectral element method (SEM) up to 2 Hz. Recently, Myers et al. (2007) clearly showed that *S*-waves are generated by shallow explosions at steep topographic relief using a combination of forward and time-reversed simulations. Further simulations and analyses will be performed to investigate these effects for the North Korean tests.

Modeling Intermediate Period (10-50 seconds) Complete Waveforms in 3D Earth Models

Improvements in topographic imaging methods and the availability of high-quality seismic data (travel times and broadband waveforms) have led to improvements in estimates in 3D seismic structure on continental and regional scales. Examples of recent 3D models include the following models: CUB2.0 (Shapiro and Ritzwoller, 2002); WENA1.0 (Pasyanos et al, 2004); Tethys (van der Lee et al., 2007); s2.9EA (Kustowski et al., 2008); JWM (Reiter and Rodi, 2008) and TX2009 (Simmons et al., 2009). These models resolve structure near the surface on 100-300 km scales and cover global (CUB2.0, S29EA, TX2009) and Eurasia (WENA1.0, Tethys, JVM). Importantly, these models are generated with different methods and data types, in many cases models are estimated from multiple data types. We seek to evaluate these models' ability to predict complete waveforms as a function of frequency. The goal being that if waveform predictions are accurate we may be able to use 3D models and simulations of complete waveforms for event analysis, such as depth determination, moment tensor estimation and yield determination. For this effort we are using the spectral element method (SEM) code SPECFEM3D (Komatitsch and Vilotte, 1998; Komatitsch and Tromp, 1999; Komatitsch et al., 2000). This code computes the response of the earth to moment tensor forcing in spherical geometry with fully 3D seismic velocity (including anisotropy) and density variations.

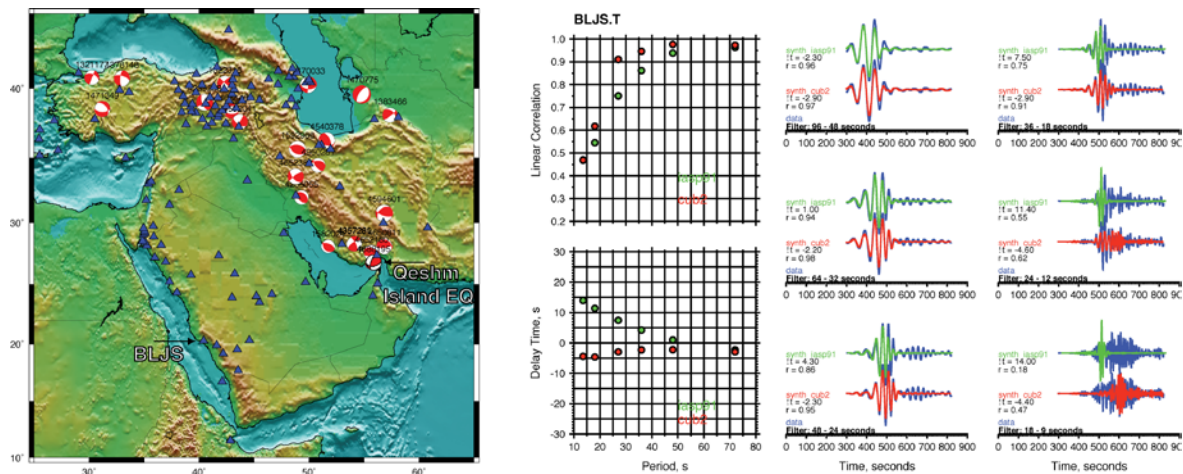


Figure 5 (a, left) Map of events (focal mechanisms) and stations for which we evaluating 3D models of the Middle East. The locations of the 11/27/2005 Qeshm Island earthquake and station BLJS (Saudi Arabia) are indicated. (b, right) Comparison of observed (blue) and synthetic waveforms for the 1D iasp91 (green) and 3D CUB2.0 (red) waveforms for the Qeshm Island events on the transverse component at station BLJS for a suite of frequency bands. Also shown are the linear correlation, *r*, and delay time, Δt , as a function of frequency.

In order to investigate the ability of current 3D models to predict complete waveforms we developed a simple method to systematically compare observed and synthetic waveforms for well-characterized events. The windowed waveform segments for a data-synthetic pair for a given event-station-channel are compared for a suite of overlapping frequency bands (9-96 seconds). At each frequency, we compute the cross-correlation and report the delay time for optimal waveform alignment and the linear correlation at the delay to reduce waveform mismatch into simple measures of timing and waveform shape, respectively.

Figure 5a shows the events and stations for which we have well-determined source parameters from Cut-and-Paste (Helmberger et al., 2008). We show only the comparison of data and synthetics for one path: the 11/27/2005 Qeshm Island, Iran (M_w 5.8) earthquake to station BLJS in southwestern Saudi Arabia. The transverse component waveforms are compared in overlapping frequency bands between 0.1-0.01 Hz (periods 9–96 seconds). Synthetics were computed for the 1D iasp91 (Kennett and Engdahl, 1991) and CUB2.0 (Shapiro and Ritzwoller, 2002) models. This particular path clearly shows how the 3D CUB2.0 model predicts the observed waveform better than the 1D iasp91 model—note that the delay time is closer to 0 (measuring phase error) and the linear correlation (measuring waveform mismatch) is larger across the period band. Note however, that there appears to be scattered surface-wave energy at late times (600-700 seconds) in the band 18–48 seconds that is not predicted by the synthetics and the waveforms are very complex in the band 9–18 seconds where neither model predicts the observed long duration.

Figure 6 shows the waveform misfit performance of the 1D iasp91 and 3D CUB2.0 models for Love waves between 18–36 seconds. The waveform misfit measurements are plotted for each event at the station location with the size proportional to the linear correlation (bigger means better waveform match) and the color according to the color scale. Note that the 3D CUB2.0 model shows markedly better predictions of the observed waveforms with the delay times on average closer to zero and the linear correlations higher than for the 1D iasp91 model (see histograms of waveform misfit). Note that the delay times for the 3D CUB2.0 model show a systematic spatial pattern that suggests how the model could be improved.

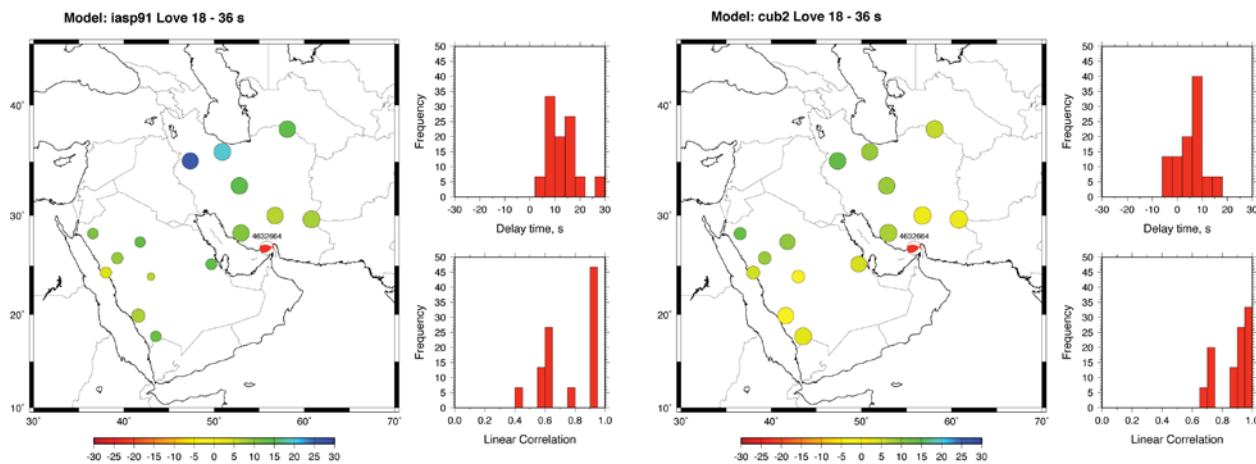


Figure 6. Maps of delay time and linear correlation for observations of the Qeshm Island earthquake Love waves in the period band 18-36 s for the 1D iasp91 (a, left) and 3D CUB2.0 (b, right) models. The waveform misfit measurements are plotted at the station location with the size proportional to the linear correlation (bigger means better waveform match) and the color according to the color-scale. Also shown are histograms of the delay times and linear correlations for each event.

Again the 2006 and 2009 North Korean nuclear tests offer important tests of 3D waveform modeling for NEM. In the previous Monitoring Research Review (Rodgers et al., 2008) we showed that the 3D wave propagation effects likely cause complexity in the BJT (Beijing, China) recordings of the 2006 North Korean nuclear test. However, this event was relatively small ($M_0 = 3 \times 10^{21}$ dyne-cm) and signal-to-noise ratios (SNR) were low. The recent May 25, 2009, nuclear test was about 6 fives larger ($M_0 = 1.8 \times 10^{22}$ dyne-cm) based on complete regional waveform modeling (Dreger et al., 2009). This provides improved SNR over the 2006 event, allowing us to investigate path effects with clearer signals.

We computed SEM synthetics for the 2009 nuclear test using the isotropic source model of Dreger et al. (2009) and three seismic models: iasp91 (Kennett and Engdahl, 1991; s2.9ea (Kustowski et al., 2008) and CUB2.0 (Shapiro and Ritzwoller (2002). Figure 7 shows the three-component waveform comparisons in the frequency band 0.02-0.05 Hz (20-50 seconds) at stations MDJ (Mudanjiang, China), INCN (Inchon, South Korea), TJN (Taejon, South Korea), BJT (Baijiatuan, China), HIA (Hailar, China) and MAJO (Matsushiro, Japan). In this period band, the iasp91 model predicts the observed response quite well with the exception of the oceanic path to MAJO. For the path to MAJO the s2.9ea model predicts the observed waveforms (distance 1144 km) very well. Note that the observed waveforms show weak but clear energy on the transverse components. Dreger et al. (2009) report that these data can be fit with a deviatoric moment tensor with significant CLVD component. Our simulations show that propagation from an isotropic source in the CUB2.0 model results in energy on the transverse component, however the amplitudes are generally weaker and the timing is inconsistent with the observations. Further investigations are needed to determine if current and future 3D models can consistently predict propagation effects and allow for unbiased source estimates.

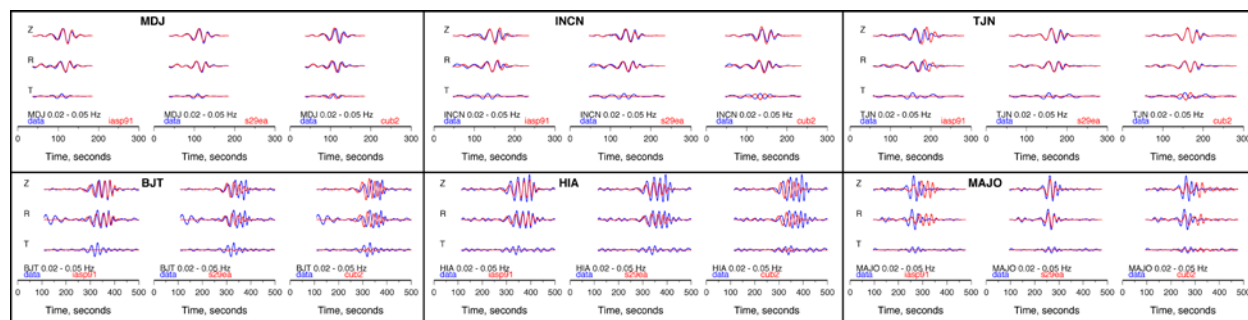


Figure 7. Comparison of observed (blue) and synthetic (red) seismograms for the May 25, 2009 North Korean nuclear test at six regional stations in the band 0.02-0.05 Hz for three models: iasp91, s2.9ea and CUB2.0 (see text). Note the upper row has a different time scale (300 seconds) than for the more distant stations shown in the lower row (500 seconds).

CONCLUSIONS AND RECOMMENDATIONS

This study shows how simulations of wave propagation in 3D earth models on high-performance computers can improve understanding and prediction of seismic observables relevant to nuclear explosion monitoring. The current efforts are focused on: 1) modeling shockwaves emerging from UNE’s in different emplacement conditions (geologies) with GEODYN and coupling GEODYN-to-WPP to propagate motions to seismic distances; 2) modeling the effect of surface topography on seismic ground motions with emphasis on the recent North Korean nuclear tests; and 3) modeling intermediate period complete waveforms at regional distances.

Specific conclusions from our shockwave modeling investigations show that the emplacement material has a strong effect on the amplitude and frequency content of seismic motions. We performed a series of fully contained 1-kiloton explosions in three canonical materials (granite, tuff and alluvium). Strong materials (granite) result in very short duration, high-amplitude and high-corner frequency motions, while weaker materials are lower amplitude and have lower corner frequency. We are currently analyzing the effect of depth-of-burial and cavity size on the character of motions. Coupling of GEODYN motions to WPP will allow us to propagate motions to local distances (< 10 km) where we will be able to model ground motion data from historical nuclear tests. This will help understand the impact of emplacement conditions and 3D structure on observed ground motions for actual nuclear tests.

We have enhanced WPP to include free-surface topography and run preliminary simulations of the 2006 and 2009 North Korean nuclear tests. The two shots were located relatively close together (< 5 km) but the simulations show significant differences in the elastic response. Notably the *P* - and *S*-waves that would ultimately propagate to teleseismic distances show azimuthal differences in the amplitudes and waveform shapes. The *P* -waves at a given azimuth show surprising differences in waveform shape for the two events that suggests that in such a region of rough topography the waveforms would decorrelate rapidly with source separation. The topography clearly causes differences in the azimuthal dependence of *S*-wave generation that would likely be revealed in differences in *S_n*, *L_g*

and possibly short-period surface wave generation. More remains to be investigated to improve understanding of how topography impacts observed waveforms in general and for these specific nuclear tests.

We are investigating the ability of 3D seismic models to predict observed regional complete waveforms at intermediate periods (10–50 seconds). The comparison of observed and simulated waveforms should be done in several frequency bands because not surprisingly the propagation is strongly frequency dependent. In the Middle East we have done preliminary comparisons of 3D model performance, but have not analyzed the performance of different models for the available events and waveforms. This type of analysis will help evaluate 3D models for waveform predictions of scenario events, moment tensor estimation using 3D synthetics and starting models for adjoint waveform tomography (Tromp et al., 2005; Savage et al., these Proceedings).

These efforts are preliminary, however results are promising and we believe they should be continued. Currently we are spending a substantial part of the effort on developing methods to accurately and efficiently run simulations. As methods evolve we will focus on comparing simulation results with data.

ACKNOWLEDGEMENTS

We thank Steve Myers for providing his joint relocations of the 2006 and 2009 North Korean nuclear tests. WPP was developed with funding from LLNL Laboratory Directed Research and Development and the Department of Energy Office of Science. We are grateful to the staff of Livermore Computing at LLNL for operating the parallel computers on which we performed many of the simulations used in this study. We also thank the LLNL Geophysical Monitoring Program Information Technology team, led by Stan Ruppert, for providing a productive computing environment that supports these efforts. SEM calculations were performed with the SPECFEM3D package developed by Jeroen Tromp, Dmitri Komatitsch and colleagues and distributed by the Computational Infrastructure for Geodynamics supported by the National Science Foundation (www.geodynamics.org).

REFERENCES

- Aagaard, B., R. W. Graves, S. Ma, S. C. Larsen, A. Rodgers, N. Anders Petersson, R. Jachens, T. M. Brocher, R. W. Simpson and D. Dreger (2009). Ground motion modeling of Hayward fault scenario earthquakes II: Simulation of long-period and broadband ground motions, manuscript in preparation, *Bull. Seism. Soc. Am.*
- Antoun, T. H., I. N. Lomov and L. A. Glenn (2001). Development and application of a strength and damage model for rock under dynamic loading, proceedings of the 38th U.S. Rock Mechanics Symposium, Rock Mechanics in the National Interest, D. Elsworth, J. Tinucci and K. Heasley (eds.), A. A. Balkema Publishers, Lisse, The Netherlands, 369–374.
- Antoun, T. H. and I. N. Lomov (2003). Simulation of a spherical wave experiment in marble using multidirectional damage model, 13th American Physical Society Topical Conference on Shock Compression of Condensed Matter, Portland, OR July 20–25, 2003.
- Boore, D. (1972). A note on the effect of simple topography on seismic SH waves, *Bull. Seismol. Soc. Am.* 62: 275–284.
- Bouchon, M. (1973). Effect of topography on surface motion, *Bull. Seismol. Soc. Am.* 63: 615–632.
- Campillo, M. and M. Bouchon (1985). Synthetic SH-seismograms in a laterally varying medium by the discrete wavenumber method. *Geophys. J. Royal Astro. Soc.* 83: 307–317.
- Chaljub, E. (2006). Spectral element modeling of 3D wave propagation in the Alpine Valey of Grenoble, France, 3rd *International Symposium on the effects of Surface Geology on Seismic Motion, Grenoble France.*
- Dreger, D., S. Ford and W. Walter (2009). Source analysis of the Memorial Day explosion, Kimchaek, North Korea, manuscript in preparation.
- Helmberger, D., A. Rodgers, S. Ni, S. Wei, and J. Tromp (2008). Advanced Waveform Simulation for Seismic Monitoring Events, in *Proceedings of the 30th Monitoring Research Review: Ground-Based Nuclear Explosion Monitoring Technologies*, LA-UR-08-05261, Vol. 1, pp. 408–418.
- Kennett, B.L.N., and E.R. Engdahl (1991). Traveltimes for global earthquake location and phase identification, *Geophys. J. Int.* 122: 429–465.
- Komatitsch, D. and J.-P. Vilotte (1998). The Spectral Element Method: An efficient tool to simulate the seismic response of 2D and 3D geologic structures, *Bull. Seismol. Soc. Am.* 88: 368–392.
- Komatitsch, D. and J. Tromp (1999). Introduction to the spectral element method for three-dimensional seismic wave propagation, *Geophys. J. Int.* 139: 806–822.

2009 Monitoring Research Review: Ground-Based Nuclear Explosion Monitoring Technologies

- Komatitsch, D., J. Ritsema and J. Tromp (2000). The Spectral-Element Method, Beowolf computing and global seismology, *Science* 298: 1737–1742.
- Kustowski B., Ekström G., and A. M. Dziewonski (2008). The shear-wave velocity structure in the upper mantle beneath Eurasia, *Geophys. J. Int.* 174: 978–992.
- Lomov. I. N., T. H. Antoun, J. Wagoner and J. Rambo (2003). Three-dimensional simulation of the Baneberry nuclear event, in Proceedings of the 13th American Physical Society Topical Conference on Shock Compression of Condensed Matter, Portland, OR July 20-25, 2003.
- Nilsson, S., N.A. Petersson, B. Sjogreen, H.-O. Kreiss (2007). Stable difference approximations for the elastic wave equation in second order formulation, *SIAM J. Numer. Anal.* 45: 1902–1936.
- Murphy, J.R., Kitov, I.O., Rimer, N., Adushkin, V.V., Barker, B.W. (1997) Seismic characteristics of cavitydecoupled explosion in limestone: An analysis of Soviet high explosive test data. *J. Geophys.Res.* 102: (12), 27393–27405.
- Myers, S., J. Wagoner, and S. Larsen (2007). Numerical experiments investigating the source of explosion *S* waves, in *Proceedings of the 29th Monitoring Research Review: Ground-Based Nuclear Explosion Monitoring Technologies*, LA-UR-07-5613, Vol. 1, pp. 175–184.
- Pasyanos, M. E., W. R. Walter, M. P. Flanagan, R. Gok, S. C. Myers, and K. M. Dyer (2007). Enhancements of geophysical models for monitoring, in *Proceedings of the 29th Monitoring Research Review: Ground-Based Nuclear Explosion Monitoring Technologies*, LA-UR-07-5613, Vol. 1, pp. 195–204.
- Perret W. R. Bass R. C. (1974). Free-field ground motion induced by underground explosions, Sandia National Laboratory Report No. SAND74-0252.
- Reiter, D. and W. Rodi (2008). A new regional 3-D velocity model for Asia from the joint inversion of *P*-wave travel times and surface-wave dispersion data, in *Proceedings of the 30th Monitoring Research Review: Ground-Based Nuclear Explosion Monitoring Technologies*, LA-UR-08-05261, Vol. 1, pp. 213–221.
- Rodgers, A., E. Matzel, M. Pasyanos, A. Petersson, B. Sjogreen, C. Bono, O. Vorobiev, T. Antoun, I. Lomov, W. Walter, and S. Myers (2008). Seismic simulations using parallel computing and three-dimensional Earthmodels to improve nuclear explosion phenomenology and monitoring, in *Proceedings of the 30th Monitoring Research Review: Ground-Based Nuclear Explosion Monitoring Technologies*, LA-UR-08-05261, Vol. 1, pp. 231–240.
- Sanchez-Sesma, F. (1983). Diffraction of elastic waves by three-dimensional surface irregularities, *Bull. Seismol. Soc. Am.* 73: 1621–1636.
- Savage, B., D. Peter, B. Covellone, A. Rodgers, and J. Tromp (2009). Progress towards next generation, waveform based three-dimensional models and metrics to improve nuclear explosion monitoring in the Middle East, these Proceedings.
- Shapiro, N.M. and M.H. Ritzwoller (2002). Monte-Carlo inversion for a global shear velocity model of the crust and upper mantle, *Geophys. J. Int.* 151: 88–105.
- Simmons, N., A. Forte and S. Grand. (2009). Joint seismic, geodynamic and mineral physical constraints on three-dimensional mantle heterogeneity: Implications for the relative importance of thermal versus compositional heterogeneity, *Geophys. J. Int.* 177: 1284–1304.
- Tromp, J., C. Tape and Q. Liu (2005). Seismic tomography, adjoint methods, time reversal and banana-doughnut kernels, *Geophys. J. Int.* 160: 195–216.
- van der Lee, S., S. Chang, M. Flanagan, H. Bedle, F. Marone, E. Matzel, M. Pasyanos, A. Rodgers, B. Romanowicz, and C. Schmid (2007). Joint inversion for 3-dimensional *S*-velocity mantle structure along the Tethyan Margin, in *Proceedings of the 29th Monitoring Research Review: Ground-Based Nuclear Explosion Monitoring Technologies*, LA-UR-07-5613, Vol. 1, pp. 312–321.
- Vorobiev. O. Y. (2008) Generic strength model for dry jointed rock masses, in press, *International Journal of Plasticity*, 10.1016/j.ijplas.2008.06.009.